Automatic detection of Vz noise and an observation of how such noise is induced

Joseph Jennings and Shuki Ronen

ABSTRACT

We develop an attribute for the automatic detection of Vz noise on OBN data. Using a 3D OBN dataset acquired in the Gulf of Mexico, we are able to show that our attribute successfully detects Vz noise and that a large shallow salt body is the primary source of this shear induced noise.

INTRODUCTION

From the early days of ocean-bottom cable acquisition, it has been known that shear waves often induce noise in ocean-bottom seismometer (OBS) data (Bagaini et al., 2000). This type of induced noise was coined the term "Vz noise" later when the same problem occurred during ocean-bottom node (OBN) acquisition (Paffenholz et al., 2006b).

While Vz noise is recorded only on the vertical geophone component, it tends to be problematic for P-wave processing. This is because it leaks on both up and down separated P-waves when the clean hydrophone data are combined with the noisy geophone data (PZ combination). While less well known, strong Vz noise can also make applications such as converted wave (PS) processing and deblending using the horizontal components significantly more difficult (Jennings and Ronen, 2017).

In order to mitigate the problem of Vz noise, two possible solutions have been discussed. One involves an acquisition solution by designing an OBS that could potentially not record the Vz noise. This solution was first indicated by the assessment performed by (Bagaini et al., 2000). They showed that one OBC group had no Vz noise and another group just 12.5 meter away had Vz noise. The analysis was that when OBC was deployed under tension, some groups were not coupled to the seabed and these tended to have Vz noise. This was later confirmed by Self Landing Ascending (SLA) OBNs data (Ronen et al., 2003). The SLA-OBN (pictured in Figure 6 of (Beaudoin et al., 2006) had an external geophone package whose deployment was triggered by the impact of the SLA-OBN on the seabed. When the seabed was too soft, the geophone package failed to deploy (this happened 5% of the time) and the external geophone package remained hanging and did not couple to the seabed. Interestingly, when this occurred, the geophone data showed strong Vz noise. However, when the external geophone was properly deployed, other nodes in the same area

had no Vz noise. This experiment indicates that there exists a potential acquisition solution to the Vz noise problem.

The other potential solution to the Vz noise problem involves a "fix it in processing" solution in which signal processing algorithms can be developed in order to separate the Vz noise from the vertical geophone component (Peng et al., 2013; Claerbout et al., 2019; Bader et al., 2019). This type of solution was first indicated by (Paffenholz et al., 2006a) where they showed that Vz noise could be explained by scattering of shear waves, regardless of OBN design. This work by (Paffenholz et al., 2006a) indicates that there might not be an acqusition solution to the Vz noise problem.

In this report, we take an opportunity to study Vz noise. Shell Exploration and Production Company (Shell) has released a full 3D GOM OBN dataset to the Stanford Exploration Project (SEP) and within SEP these data are currently being used for testing various processing and imaging methods under development, including deblending. During our initial processing of the data, we found that some nodes had strong Vz noise and some were completely clean. We found that in general, nodes deployed over shallow salt had Vz noise while nodes far away from the salt did not.

Given that in these data all of the nodes are of the same type, what we found seems to confirm the claim made by (Paffenholz et al., 2006a). However, we found that some nodes near the salt did not have Vz noise and that the Vz noise varied between neighboring nodes with a spacing of 400 m.

DATA AND METHOD

SEP received a 3D GOM OBN dataset from Shell during the summer of 2017. Within SEP, these data have been used for testing imaging, velocity model building and geophysical signal processing algorithms (Dahlke, 2019; Wang et al., 2019). The data consist of 23,241 shots and 916 OBNs . Figure 1 shows source and receiver positions plotted on a depth slice of a 3D RTM image provided by Shell.

The depth slice shown in Figure 1a shows the presence of a large circular salt body at approximately 15 km in the inline direction and 15 km in the crossline direction. Near the salt body, positioned at approximately 12 km in the inline direction and 16 km in the crossline direction is positioned a platform. This platform is the cause for the small gap in shot points near the salt body.

Figure 2 shows three nodes and two shot lines nodes plotted on a windowed portion of the depth slice. The data from these nodes will be shown throughout this report. Figure 3 shows the raw four-component data from the node closest to the salt indicated by the red marker in Figure 2. Note that on each of the geophone components, there appears events that are strong in amplitude and have lower frequency content than the proceeding reflections. These events are denoted as Vz noise and will leak into the up and down-going data after PZ summation.

In our initial exploration of these data, we discovered that more than just this par-

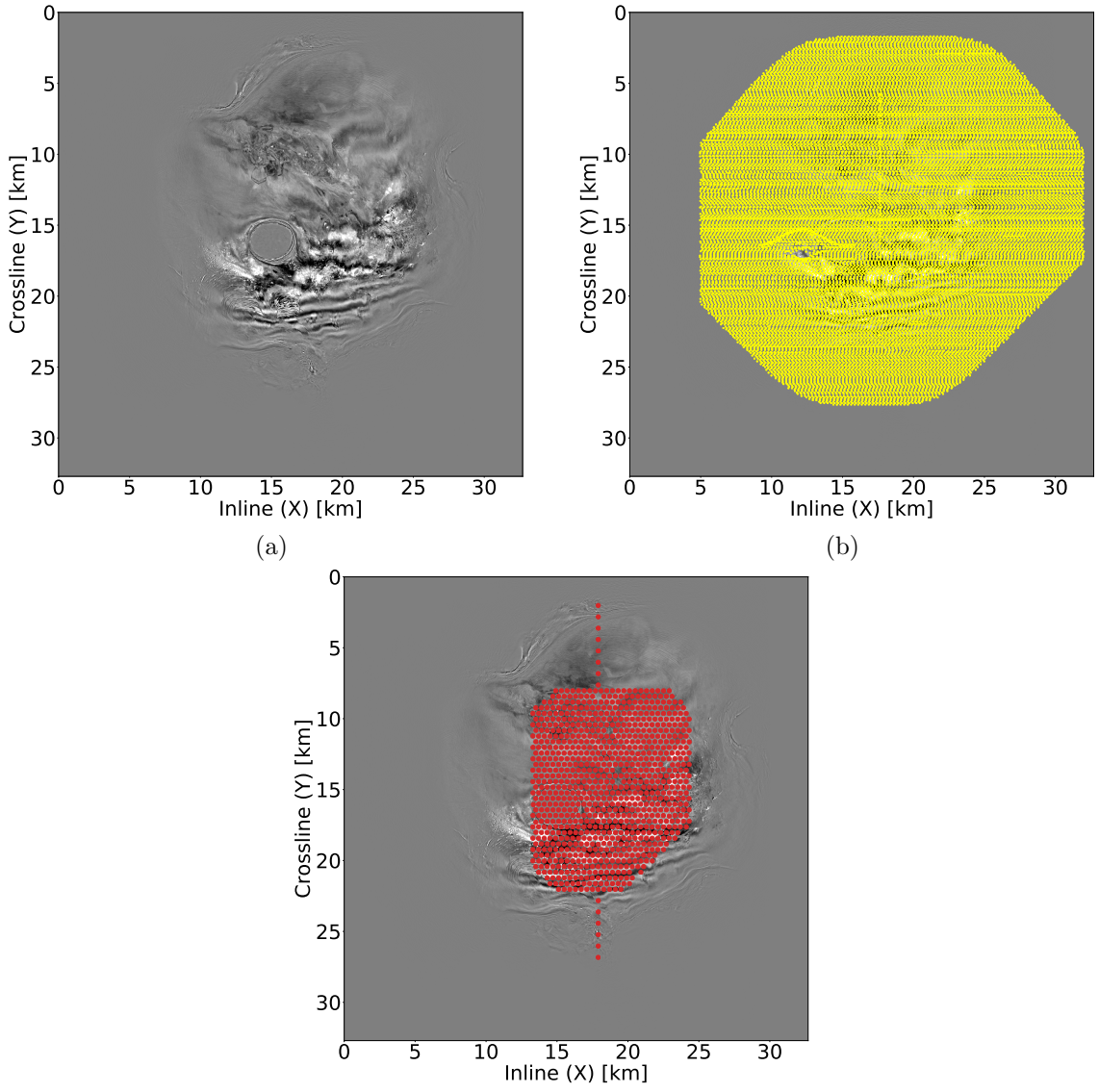


Figure 1: (a) Depth slice taken at 1.24 km depth, (b) shot positions, (c) receiver positions. [**CR**]

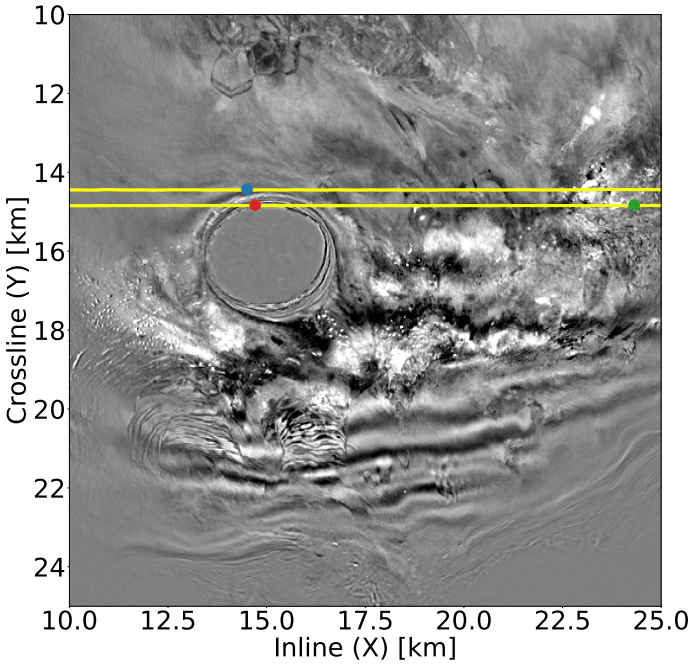


Figure 2: Three nodes and two shot lines used for analyzing Vz noise. [**CR**]

ticular node contained Vz noise and we felt the need to automatically identify nodes that contain Vz noise and those that do not. To carry out this task, we developed a scalar attribute whose strength indicates how much Vz noise is present on a particular node. We calculate this attribute on the vertical component of each node in the following manner:

1. Window out only a line of shots that were acquired directly over the node
2. Apply a hyperbolic moveout correction (HMO) to the line in order to flatten the direct arrival and the bubble
3. Apply a high-cut filter of maximum 80 Hz to remove the higher frequency signal and leave the lower frequency noise
4. Window the line of shots in time from two seconds to seven seconds
5. Window the line of shots again so that the maximum offset is 4 km
6. Lastly, calculate the energy of the data within this chosen window

Figure 4 shows the windowed, moveout corrected and filtered vertical component data used from the node shown in Figure 3 to calculate the energy of the Vz noise. For this particular gather, the our normalized attribute calculation is of about magnitude 1.0. For a clean gather we typically found that our attribute reported values on the order of 0.001 (1000 times less). While we admit it would be better to use more than just

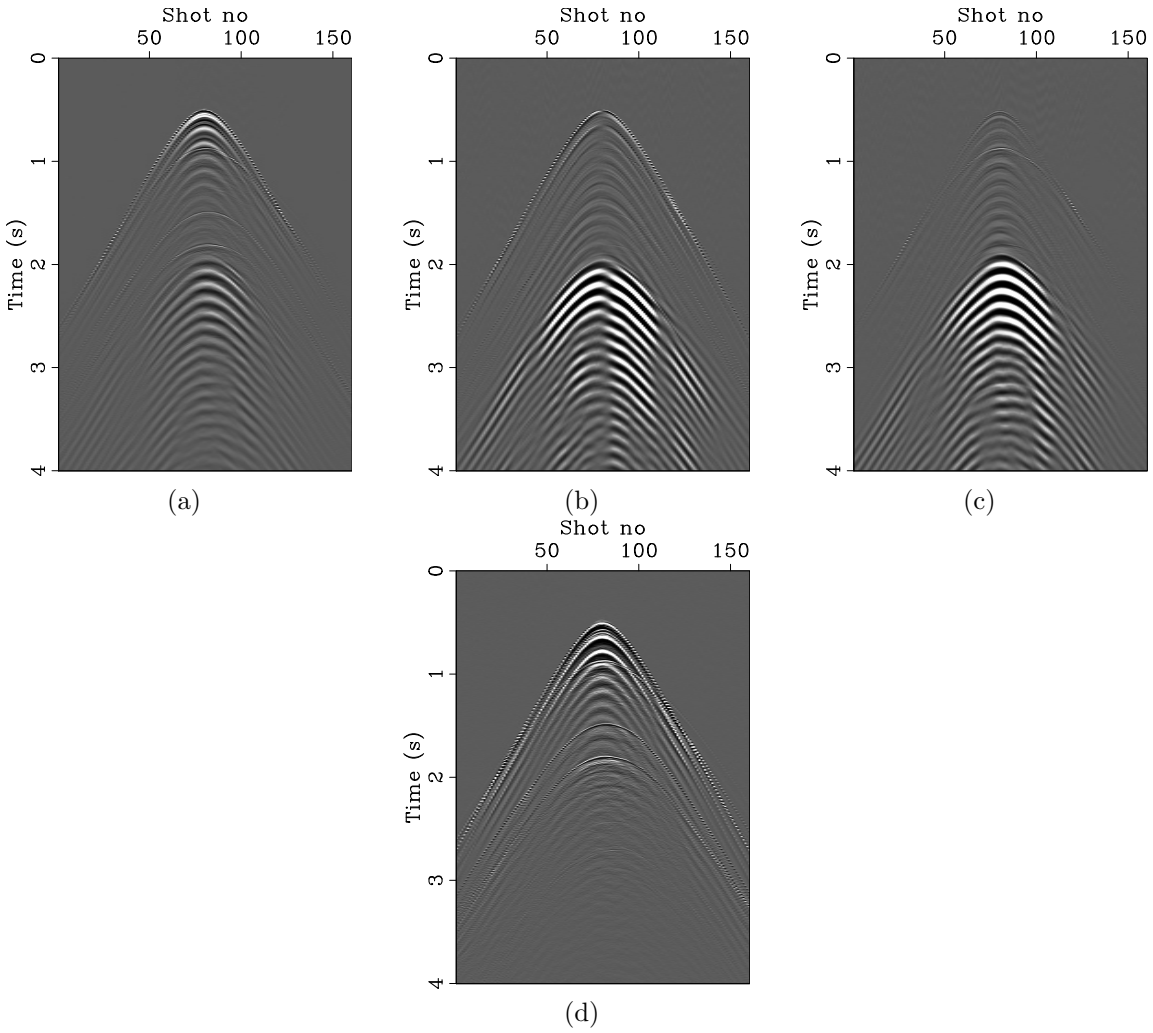


Figure 3: Raw multicomponent data from the node nearest the salt shown in Figure 2. (a) Vertical component, (b) inline component, (c) crossline component and (d) hydrophone component. Note that when comparing the vertical and hydrophone components, while the higher frequency reflections from the water bottom and the top of salt are seen in both panels, the vertical contains strong low-frequency events starting at approximately 2 s. These events are shear induced events and are called Vz noise. Note also these events appear quite strong on both the inline and crossline horizontal components. [**CR**]

a 2D line for this calculation in order to capture effects of 3D wave propagation and scattering, the results in the following section seem to show that this is not necessary.

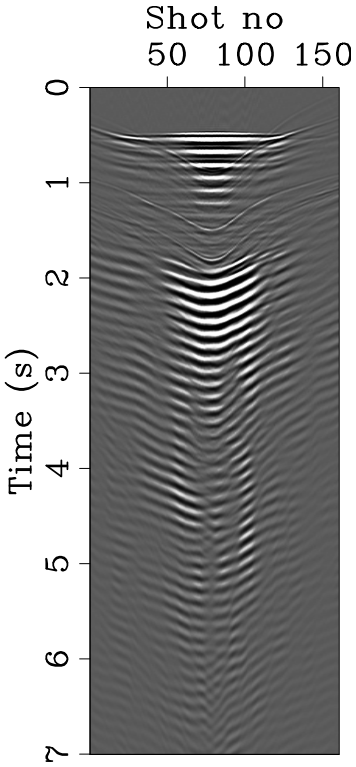


Figure 4: An example of a windowed, moveout corrected and filtered vertical component gather used for our attribute calculation. The data are squared and summed from two to seven seconds to calculate the energy within that window. Note that for this particular gather the Vz noise completely dominated within this two to seven second window. [**CR**]

RESULTS

The application of our attribute calculation for each node is shown in Figures 5 and 6. As the colorbar indicates $-20 \log$ attribute (something like dB), the red colors indicate nodes with more Vz noise and the green colors indicate nodes with little to no Vz noise. The superposition of our node map on the depth slice indicates that the the nodes that contain the highest amount of Vz noise are located near the large salt body. In fact, there exists a sharp transition between clean and noisy nodes at the salt boundary unmistakably indicating that the salt body is responsible for the induced shear noise on the vertical components of the OBNs. While we are uncertain of the exact mechanism of how this induced shear noise is generated, we suspect that the salt body acts as a large scatterer that radiates Scholte waves which propagate along the seafloor and then are induced on the vertical component of the OBN.

In order to verify our attribute calculation, we display the data from the three nodes shown in Figure 2 after both NMO and HMO applied. The application of NMO provides a display of the mirror image of the seabed and the application of HMO allows us to distinguish between the moveout of the bubble and the moveout the shear induced noise. Figure 7 shows NMO applied to the data from the node indicated by the red marker (closest to the salt). Note that starting at approximately 2 s significant

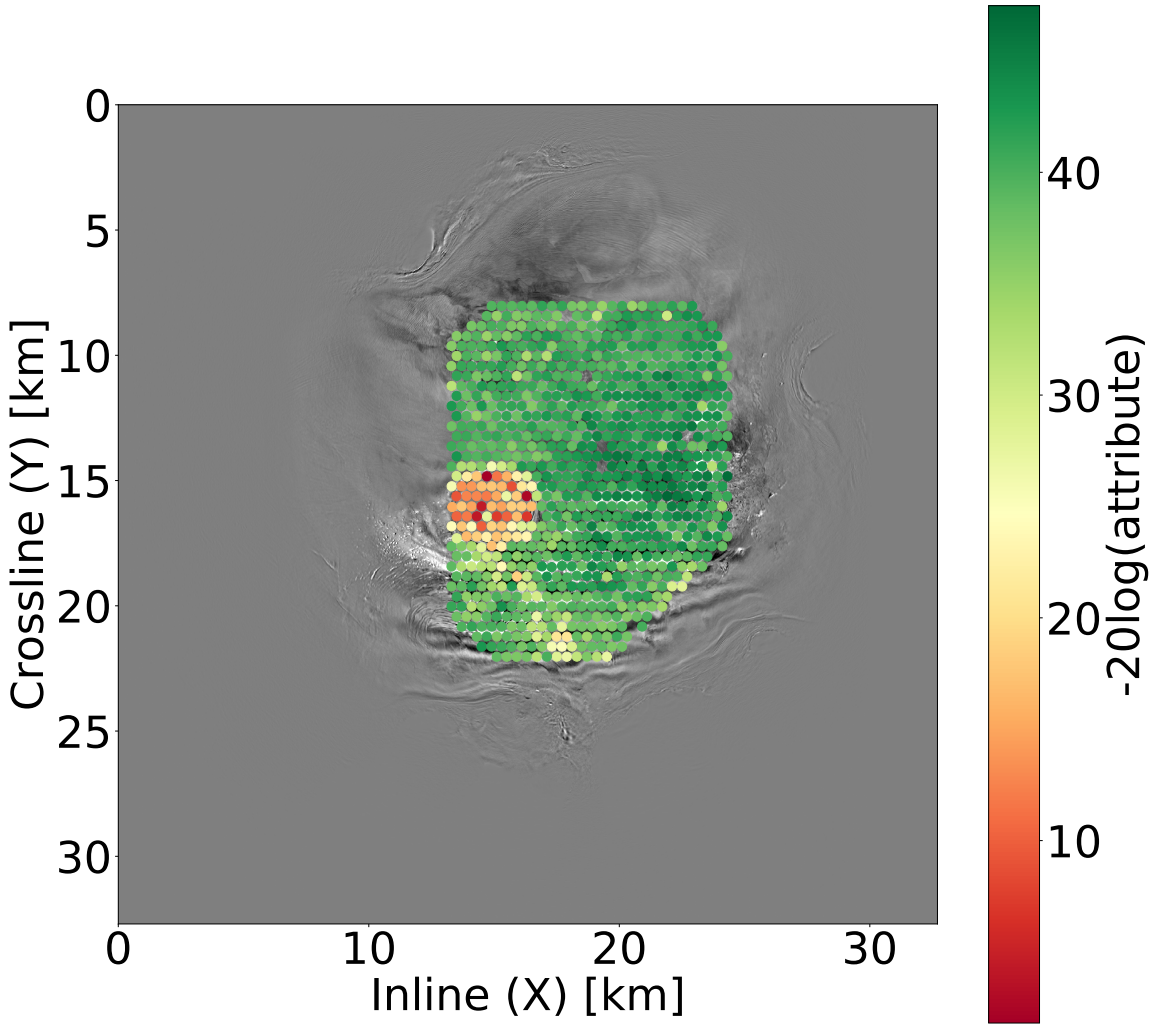


Figure 5: Calculation of the Vz noise attribute for each node. Each colored dot represents a node and the color of the node the strength of the Vz noise. Green colors indicate less Vz noise and red colors inidicate higher amounts of Vz noise. A large circular region of nodes with high Vz noise are positioned directly over the salt body. [**ER**]

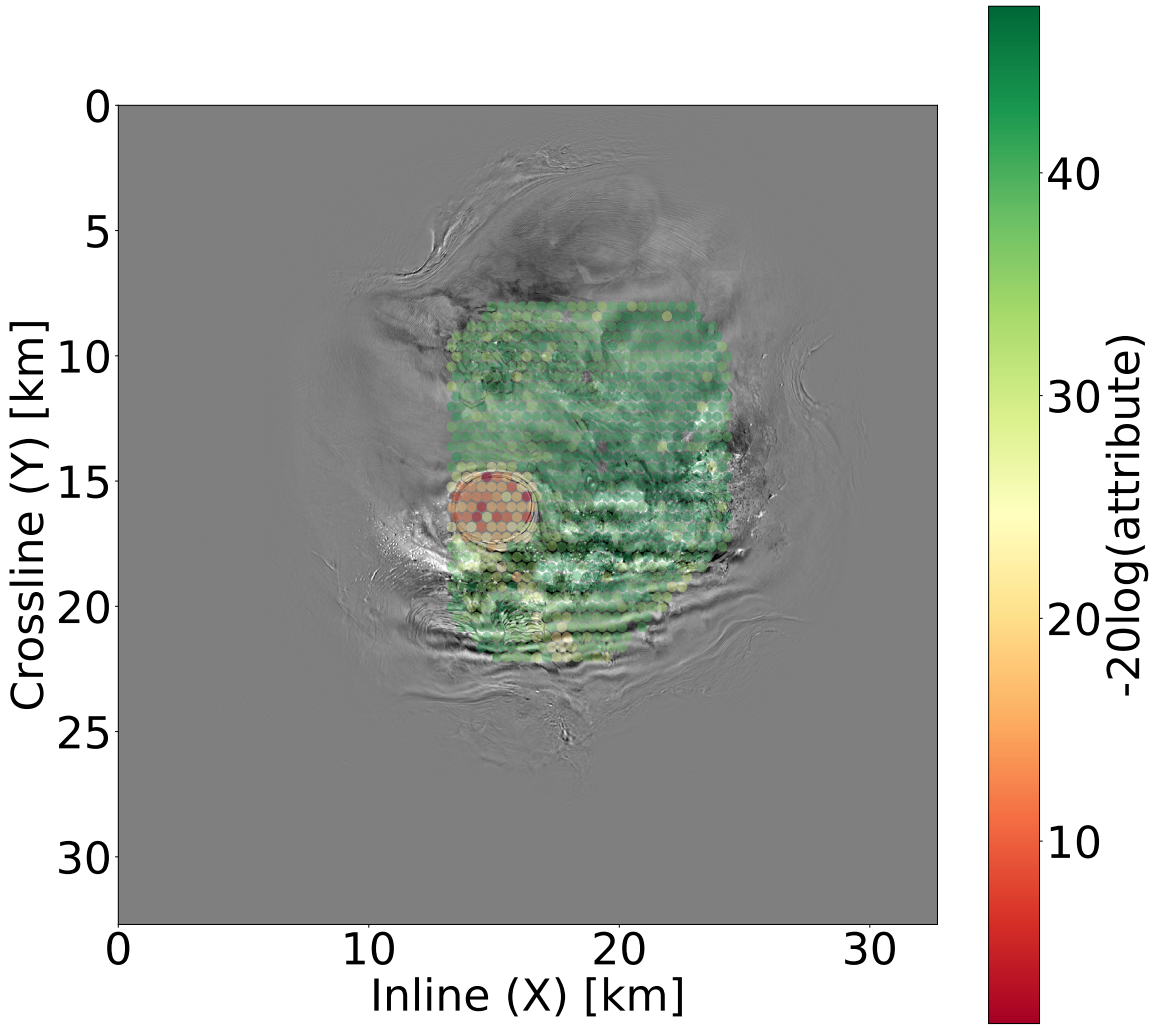


Figure 6: The same as Figure 5 but the nodes are now plotted with a slight transparency making it readily apparent that the high Vz noise nodes are positioned over the salt body. [**ER**]

amounts of Vz noise can be observed as high amplitude low frequency events. While these events appear on each of the geophone components, they do not appear on the hydrophone component. Figure 8 shows the application of NMO applied to the node indicated by the blue marker shown in Figure 2. The Vz noise is much milder on this node (as is indicated by the light green color on Figures 5 and 6) and can be seen at approximately 2.6 s. Again this Vz noise corresponds to high amplitude shear events that are readily seen on both the inline and the crossline components. Lastly, we display the data from the node indicated by the green marker shown in Figure 2. Note that as this node is far from the salt, it has almost no Vz noise as is indicated by Figures 5 and 6. This is clearly evident when comparing the hydrophone and vertical components shown in Figures 9a and 9d as they appear highly correlated (which is desired for a successful PZ combination for up down separation).

Figures 10 - 11 show the result of HMO applied to these data. Note that as the bubble and the Vz noise have similar frequency content and in some cases similar amplitudes, they can be difficult to distinguish. HMO will flatten the bubble but not the recorded shear events making it easier to distinguish between the two. This is clear in Figures 10 and 11 where the bubble is clearly flat (seen from approximately 0.5 - 1s) and the induced shear noise is overcorrected (seen below 2 s).

CONCLUSION

It has been shown in the past that VZ noise can come from either poor coupling or from scattering of shear waves converted to surface waves recorded by well coupled OBNs. In this paper, we found that such conversion seems to be happening by shallow salt. The fact that some nodes near the salt had VZ noise and neighboring nodes did not, can perhaps be explained by the variable seabed rigidity. It is known that earthquake damage is more severe when the ground is soft (Mexico City 1985, Wikipedia). It was found there that "Damage to structures is worsened by soil liquefaction ...". We speculate that similarly, seabed condition, probably rigidity, is possibly a third factor to coupling and shallow scatters.

ACKNOWLEDGEMENTS

We thank Shell Exploration and Production for providing the 3D GOM OBN dataset used in this study.

REFERENCES

Bader, M., R. Clapp, and B. Biondi, 2019, Low frequency de-noising using high frequency prediction error filters, *in* SEG Technical Program Expanded Abstracts 2019: Society of Exploration Geophysicists, 4500–4504.

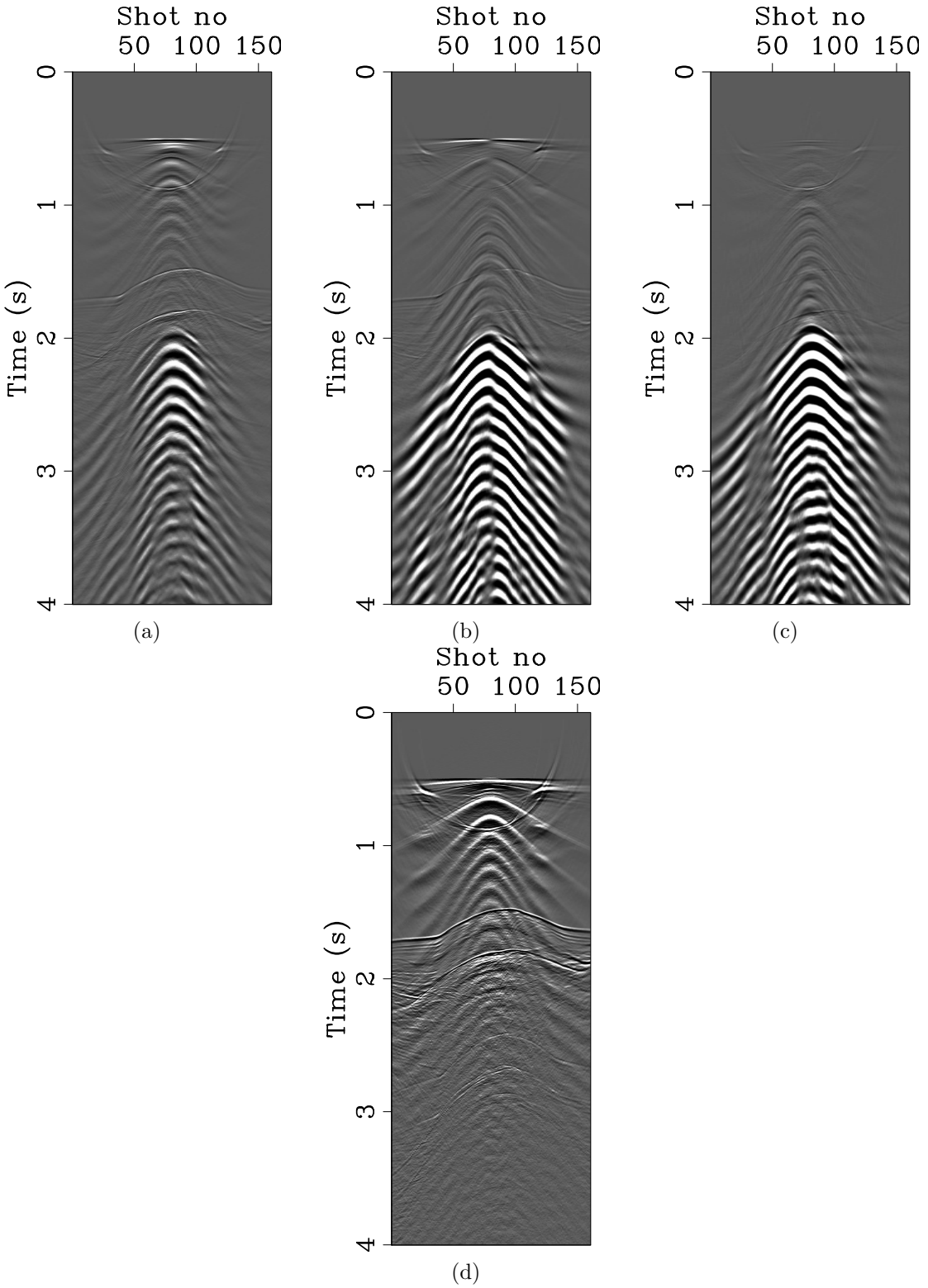


Figure 7: NMO applied to a node containing high Vz noise positioned near the salt body (the red marker shown in Figure 2. (a) Vertical component (b) inline component, (c) crossline component and (d) hydrophone component. Note that starting at approximately two seconds the Vz noise can be seen as high-energy low frequency arrivals on the geophone components. [**CR**]

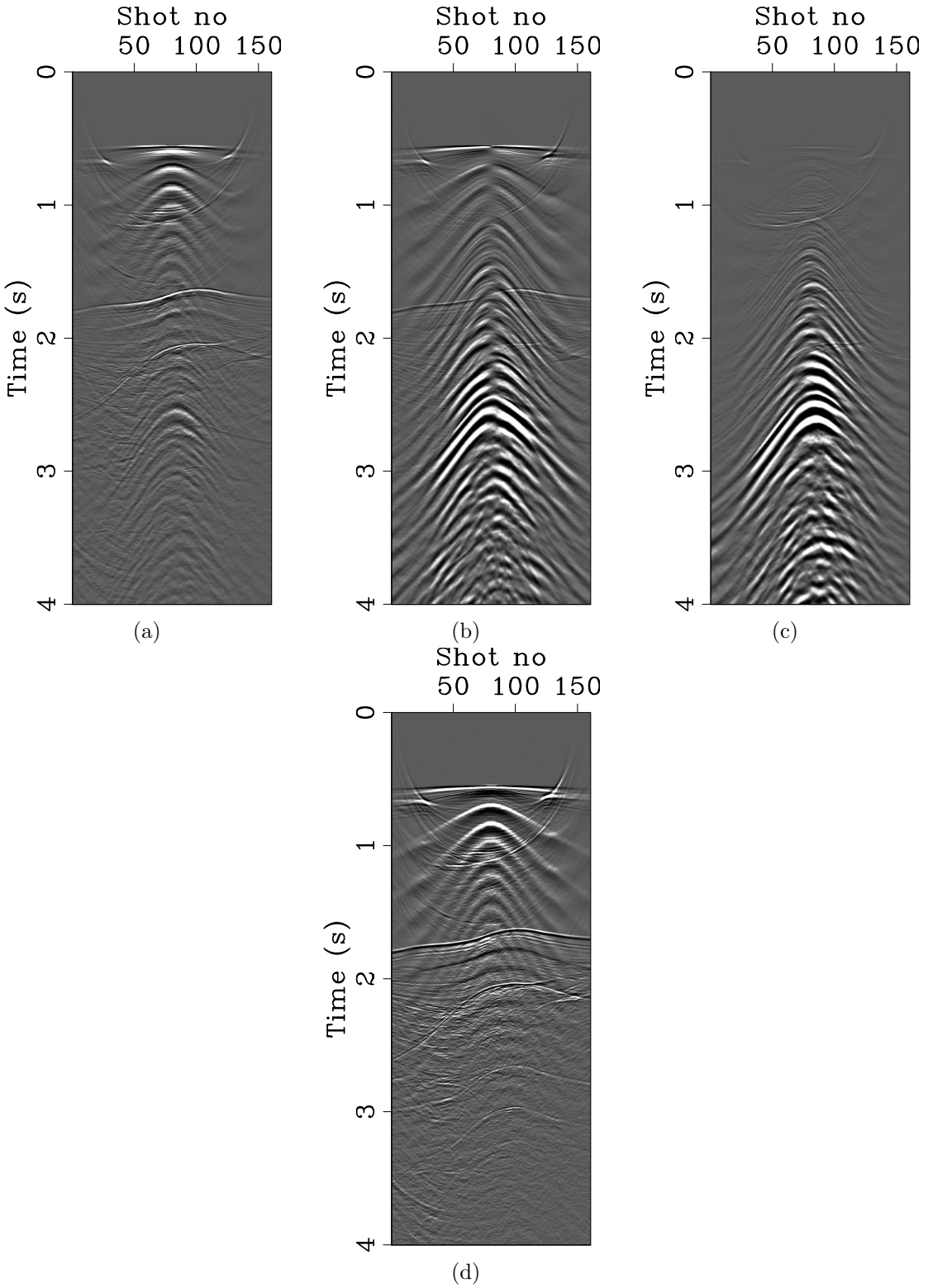


Figure 8: NMO applied to a node containing a mild amount of Vz noise also positioned near the salt body (the blue marker on Figure 2). (a) Vertical component, (b) inline component, (c) crossline component and (d) hydrophone component. The presence of mild Vz noise can be observed starting at approximately 2.5 s. [**CR**]

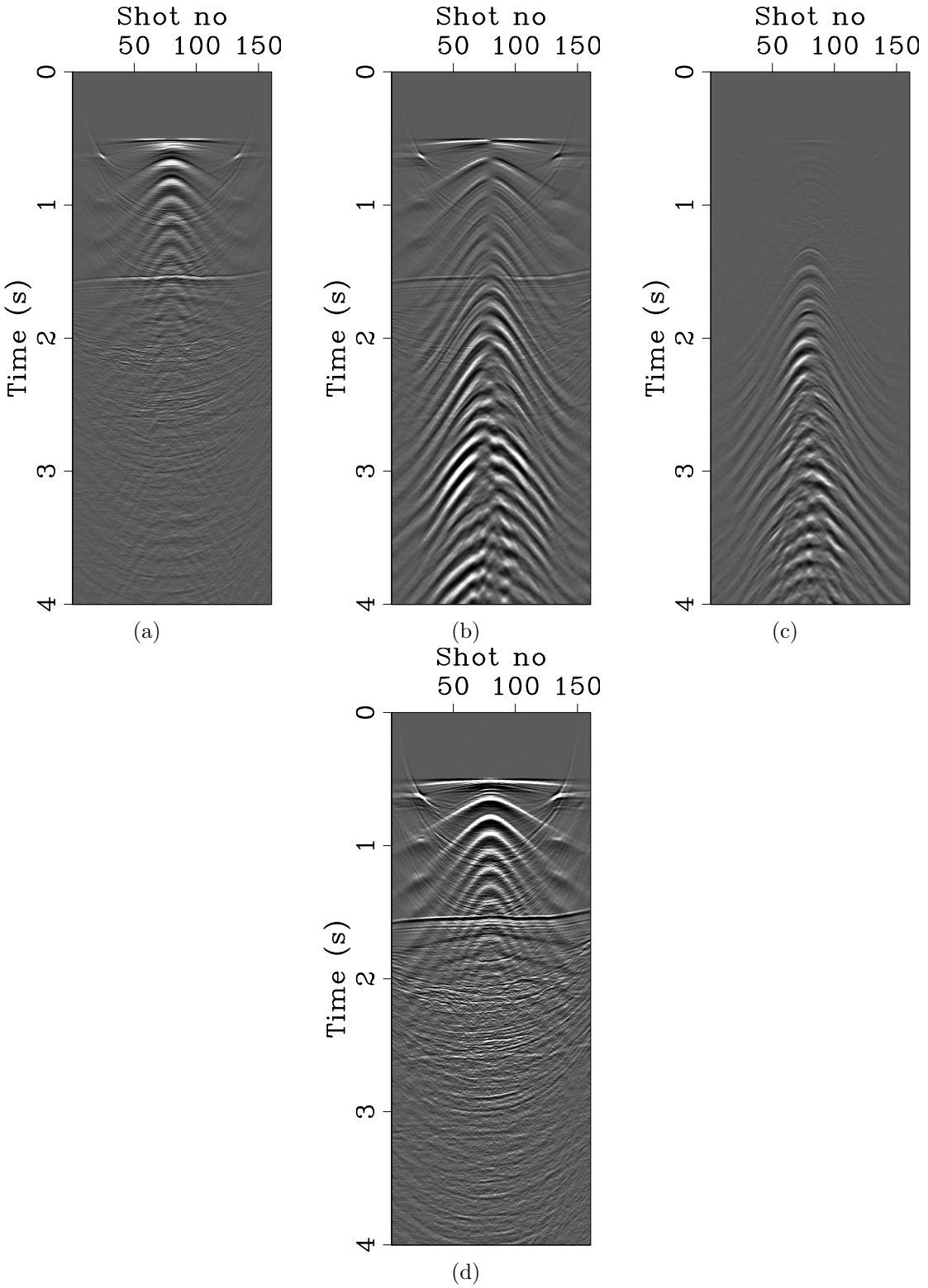


Figure 9: NMO applied to a node containing no Vz noise and positioned far from the salt (the green shown in Figure 2). (a) Vertical component (b) inline component, (c) crossline component and (d) hydrophone component. Note that the vertical and hydrophone components appear quite similar as to be expected when small amounts of Vz noise are present. [**CR**]

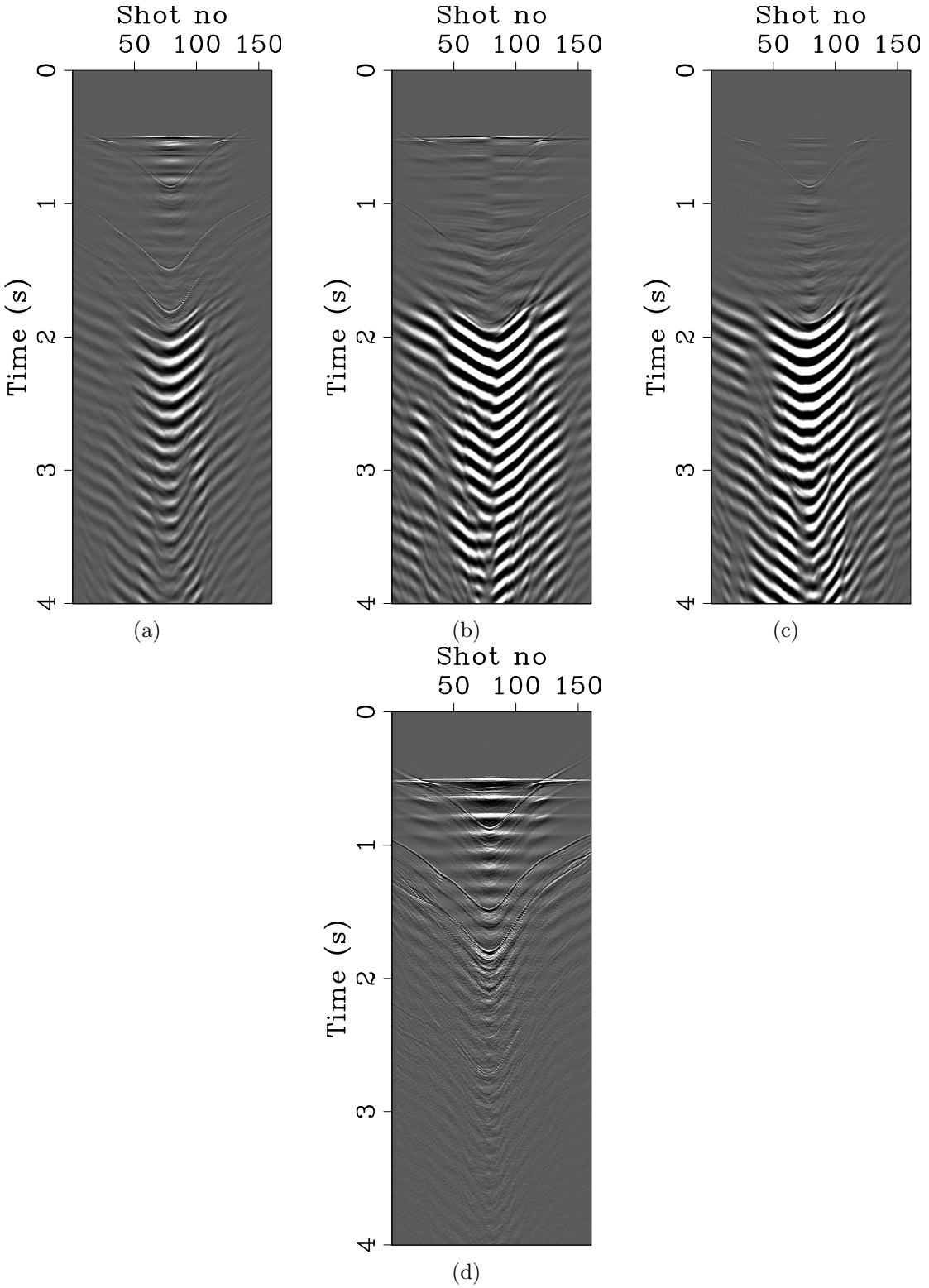


Figure 10: HMO applied to the data shown in Figure 7. Note that the bubble is flat but the Vz noise is not allowing us to distinguish between the two events. [**CR**]

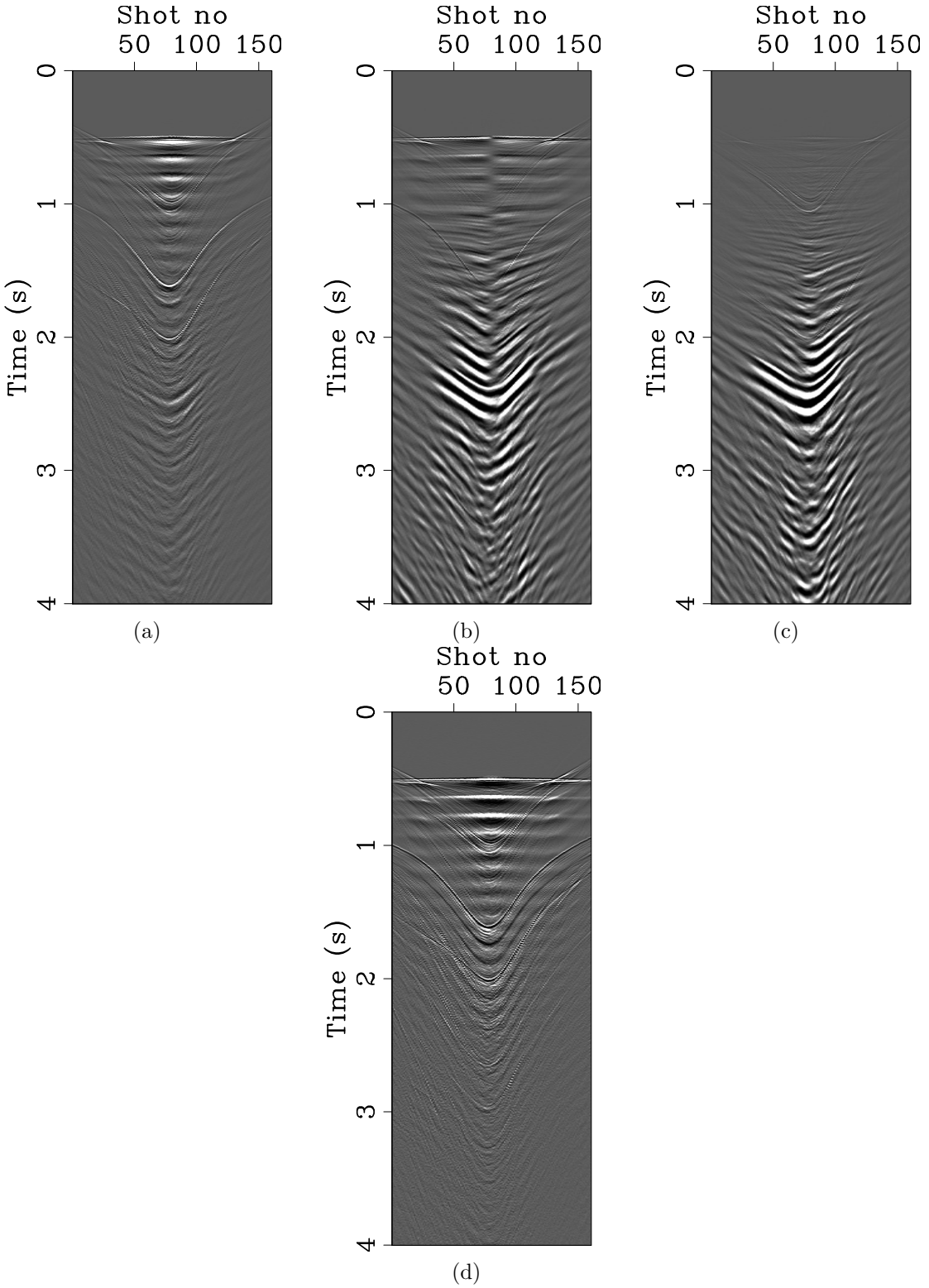


Figure 11: HMO applied to the data shown in Figure 8. [**CR**]

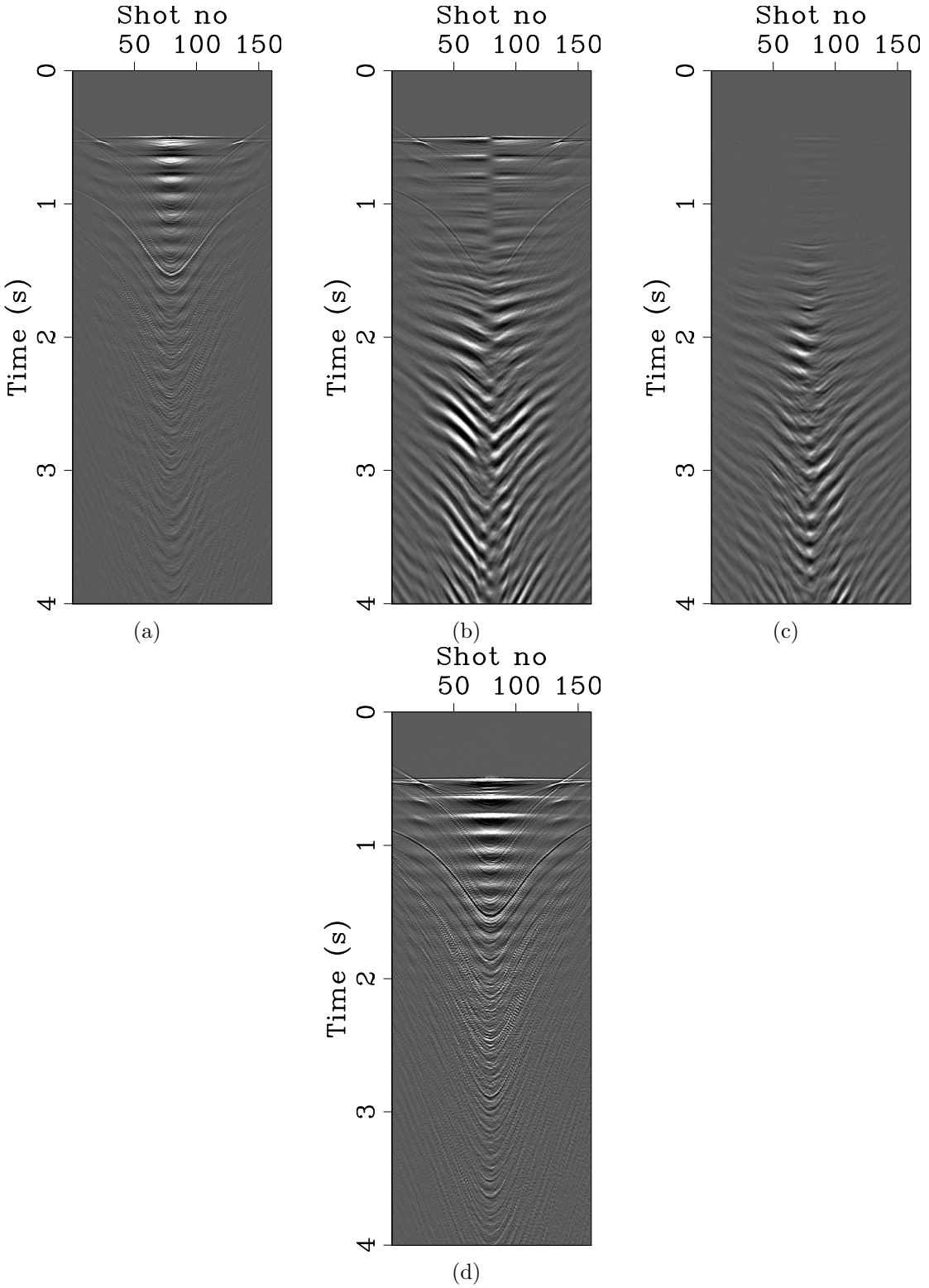


Figure 12: HMO applied to the data shown in Figure 9. [**CR**]

Bagaini, C., R. Bale, P. Caprioli, E. Muyzert, and S. Ronen, 2000, Assessment and calibration of horizontal geophone fidelity in seabed-4c using shear waves: Presented at the 62nd EAGE Conference & Exhibition.

Beaudoin, G., S. Michell, et al., 2006, The atlantis obs project: Obs nodes-defining the need, selecting the technology, and demonstrating the solution: Presented at the Offshore Technology Conference, Offshore Technology Conference.

Claerbout, J., A. Guitton, S. Levin, and K. Wang, 2019, Data fitting with non-stationary statistics.

Dahlke, T., 2019, Velocity model building using shape optimization applied to level sets: PhD thesis.

Jennings, J., and S. Ronen, 2017, Simultaneous source deblending with the radiality and source-similarity attributes: Presented at the 2017 SEG International Exposition and Annual Meeting, Society of Exploration Geophysicists.

Paffenholz, J., P. Docherty, R. Shurtleff, and D. Hays, 2006a, Shear wave noise on obs vz data-part ii elastic modeling of scatterers in the seabed: Presented at the 68th EAGE Conference and Exhibition.

Paffenholz, J., R. Shurtleff, D. Hays, and P. Docherty, 2006b, Shear wave noise on obs vz data-part i evidence from field data: Presented at the 68th EAGE Conference and Exhibition.

Peng, C., R. Huang, and B. Asmerom, 2013, Shear noise attenuation and pz matching for obn data with a new scheme of complex wavelet transform: Presented at the 75th EAGE Conference & Exhibition incorporating SPE EUROPEC 2013.

Ronen, S., A. Ratcliffe, P. Nichols, K. Mills, R. Leggott, K. Hawkins, and L. Scott, 2003, Combined ocean bottom stations and surface towed seismic streamers: Presented at the 65th EAGE Conference & Exhibition.

Wang, K., J. Jennings, and J. Claerbout, 2019, Up-down separation and debubble using a multicomponent non-stationary prediction-error filter, *in* SEG Technical Program Expanded Abstracts 2019: Society of Exploration Geophysicists, 4605–4609.